showing the high quality of the data. The mirroring is explored in Fig. 1d, by plotting the mean value or baseline

$$\mathrm{BL} = \frac{\mathrm{PECD}_R - \mathrm{PECD}_S}{2}.$$

Deviation from the ideal value of zero could be ascribed to statistical error (different S/N), to systematic error (*e.g.* residual instrumental asymmetry), or to different enantiopurity. In the higher resolution PES recorded by Rennie *et al.*[51] with a hemispherical analyzer the electronic band structure is slightly more marked and seen to correlate with the PECD changes. The OVGF calculations published by Rennie *et al.* also correspond to the observed oscillations, which highlights the enhanced sensitivity of PECD to electronic structure when compared to usual observables such as ionization cross-sections—even in the case of congested electronic bands as already observed in camphor[36] and glycidol.[13]

The onset of camphor parent ion fragmentation is ~9.7 eV, with the parent ion rapidly disappearing as photon energy is increased (less than 10% of parent yield remains at 10.0 eV). The first electronic band seen in Fig. 1c, which corresponds to ionization of the HOMO orbital localized onto the carbonyl oxygen lone pair, results solely in the production of parent ion. Thus, by filtering the electron images according to the coincident parent ion mass, the electrons ejected from the HOMO can be better isolated. This becomes[36] extremely useful at high photon energies where the moderate resolution of the VMI leads to overlap between the HOMO and the inner orbital bands. Fig. 2 illustrates the result of applying the filtering for the parent ions at $h\nu$ = 12.3 eV, and can be directly compared to Fig. 1. It is clear that the mass-filtering removes the contribution from inner orbitals since these lead to fragmentation. Conversely, to obtain the PECD of the deeper-lying orbitals, we have obtained the electron images correlated to the fragment ions only, so ensuring removal of any contribution from the HOMO orbital electron data. This treatment is especially effective when the HOMO and HOMO−1 orbitals have b_1 parameters of opposite sign, and so might tend to cancel if unresolved, as happens here in certain regions of photon energy. For instance, at $h\nu$ = 12.3 eV the weighted HOMO $|b_1|$ values obtained from Fig. 1c (unfiltered) and Fig. 2 (filtered) are 0.055 and 0.058, respectively, a discrepancy in the unfiltered data of 5% due to the small overlap between HOMO and HOMO−1.

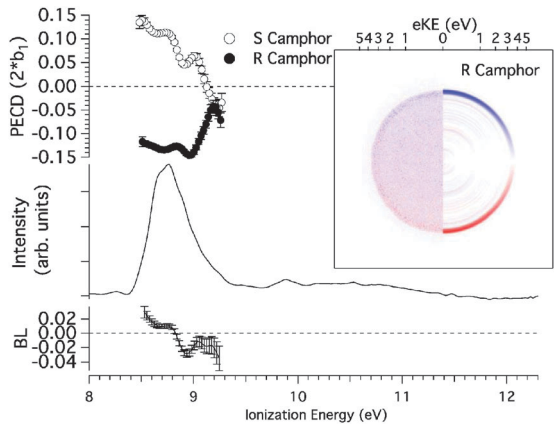

Fig. 2 PECD (open and filled circles) and PES (solid line) extracted in coincidence with parent ions (*m*/*z* 152, plus 153 and 154 to take into account the ^{13}C contributions) recorded for 1*R*,4*R*- and 1*S*,4*S*-camphor at $h\nu$ = 12.3 eV. The data have been normalized by S_3 and the ee measured by GC × GC-TOFMS. The bottom-left axis represents the PECD baseline (BL) extracted as the mean value of the *R* and *S* PECD curves. The inset shows the raw (left) and Abel inverted (right) difference image for 1*R*,4*R*-camphor corresponding only to photoelectrons correlated to parent ions.

In addition, the double imaging coincidence scheme permits removing common background impurities such as water, N_2, O_2, which would increase the achiral content in the total signal used for normalization and therefore decrease the observed PECD. Overall, the procedure dramatically increases the signal-to-noise ratio with respect to previous non-coincident data[36,40] recorded for camphor and fenchone, as evidenced with the low error bars and excellent mirror behavior. Indeed, in Fig. 1c the PECD baseline, BL, barely deviates from the ideal zero value over the whole kinetic energy range, with a weighted mean value of 0.0003 ± 0.0005. Deviations from zero outside of the given error bars are ascribed to systematic errors. It is worth noting that the *R* and *S* measurements correspond to two different experiments spaced by one month. In Fig. 2, the parent-coincident data show small deviations from perfect mirroring behavior, associated to the lower overall signal. Even in this case, however, the PES intensity weighted integral of the baseline, BL, over the FHWM of the HOMO band is very close to zero, 0.0005, so that the mean b_1 values across the HOMO and HOMO−1 regions (see text below and Fig. 3 and 4) will have very similar absolute values for both enantiomers within the given error bars—provided both have the same enantiopurity.

However, at the photon energies where both enantiomers were recorded (12.3 and 15.0 eV), we initially found that the raw, uncorrected magnitude of the HOMO band PECD measured for the *R* enantiomer was slightly smaller than that of the *S*, leading to a $\mathrm{PECD}_R/\mathrm{PECD}_S$ average ratio of 0.97 ± 0.02, as derived from the uncorrected data presented in Fig. S1(a) (ESI†). It is known that the magnitude of measured asymmetries will scale linearly with the absolute value of the enantiomeric excess (ee) as defined by ([R] − [S])/([R] + [S]) where [R] (resp. [S]) corresponds to the concentration of the R (resp. S) enantiomer, and this therefore suggests some variation of the relative enantiopurity of the two commercial samples with an ee ratio of 0.97 ± 0.02, surprisingly quite different from the value of 1.02 that could be inferred from the optical rotation data provided by Aldrich (see Experimental methods above). We therefore took additional steps to verify purity of our samples analyzing them by chiral-sensitive GC × GC-TOFMS to obtain a precise value of the ee. The results of the chromatographic analysis are shown in Table 1. The agreement between ee ratio deduced from these PECD data and the absolute ee obtained by GC × GC-TOFMS is remarkable, as are the experimental PECD error bars. The presented data of Fig. 1, and that discussed further below discussed were subsequently corrected for these reduced ee ratios, to represent the enantiopure values for PECD.

The importance of the quality of the circular polarization needs also to be highlighted because the measured b_1 is directly